Speed limit of protein folding evidenced in secondary structure dynamics

Milo M. Lin[a], Omar F. Mohammed[a], Gouri S. Jas[b], and Ahmed H. Zewail[a,1]

[a]Physical Biology Center for Ultrafast Science and Technology, Arthur Amos Noyes Laboratory of Chemical Physics, California Institute of Technology, Pasadena, CA 91125; and [b]Department of Chemistry, Biochemistry, and Institute of Biomedical Studies, Baylor University, Waco, TX 76706

Contributed by Ahmed H. Zewail, August 22, 2011 (sent for review August 4, 2011)

As the simplest and most prevalent motif of protein folding, α-helix initiation is the starting point of macromolecular complexity. In this work, helix initiation was directly measured via ultrafast temperature-jump spectroscopy on the smallest possible helix nucleus for which only the first turn is formed. The rate's dependence on sequence, length, and temperature reveals the fastest possible events in protein folding dynamics, and it was possible to separate the rate-limiting torsional (conformational) diffusion from the fast annealing of the helix. An analytic coarse-grained model for this process, which predicts the initiation rate as a function of temperature, confirms this picture. Moreover, the stipulations of the model were verified by ensemble-converging all-atom molecular dynamics simulations, which reproduced both the picosecond annealing and the nanosecond diffusion processes observed experimentally.

nucleation | time-resolved fluorescence | macromolecules | refolding

Although biomolecular systems necessarily contain many degrees of freedom, this alone is not sufficient to account for their complexity. Rather, cooperative interaction of the constituents is the defining feature at all levels of biomolecular folding and function. This complexity in protein thermodynamics and dynamics can be represented as a multidimensional free energy landscape through which the protein traverses a multitude of folding pathways funneling to the native state (1–6). Due to the interplay of entropic search and enthalpic trapping in kinetically stable intermediates, this folding process ranges in timescale from hundreds of nanoseconds to minutes depending on the protein size and sequence (3), and methods for predicting such rates, preferably in analytic expressions, are needed.

As one of the three types of polypeptide secondary structure, the α-helix is a basic and ubiquitous feature of protein structure and a key component of protein folding (1–6). In addition, because the helix is stabilized by hydrogen bonds between residues i and $i+4$ along the polypeptide backbone, the formation of the first turn (helix initiation) requires the proper arrangement of three sets of torsion angles to achieve the correct conformation for completion of the hydrogen bond. Depending on the side chains, orientation of some torsional angles may sterically restrict the movement of other angles. Thus, helix initiation is the most basic cooperative process to study. As such, it serves as a benchmark system for elucidating generic features of secondary structure formation and their possible roles in the folding process.

Here, we utilize the relative simplicity of this basic motif and examine its dynamic folding/unfolding. Ultrafast temperature-jump (T-jump) spectroscopy, analytical modeling, and ensemble-level all-atom simulations are employed to give a full picture of this process. Importantly, a representative energy landscape can be constructed in three dimensions, showing that, despite its relative simplicity, helix initiation has the common features of the funnel-type picture (1) of protein folding. One of the most significant findings, both experimentally and theoretically, is the sequence- and length-dependent separation of timescales between cooperative annealing and torsional diffusion, as well as between helix initiation and propagation.

For long polypeptides, the entire helix formation process has also been measured and found to occur in hundreds of nanoseconds (7–9). The multiple possible initiation sites along the peptide, in conjunction with helix propagation, give rise to the overall helix formation timescale, which is dependent on the sequence, temperature, and helix length. Hence, for these long polypeptides, the elementary steps of helix nucleation are convoluted by propagation and other processes that dominate the dynamics. Molecular dynamics (MD) simulations predict that helix initiation occurs on timescales ranging from hundreds of picoseconds to a few nanoseconds for short α-helical polypeptides (10–12), and such timescales are not experimentally accessible to fast T-jump studies, being limited to 10–20 ns temporal resolution (2, 7–9, 13–18). With the ultrafast T-jump methodology of this laboratory (19, 20), we have been able to study ultrafast processes of helix initiation (21). However, the rates per se do not provide the full picture for the landscape of folding.

In this contribution, we present studies of sequence and temperature dependencies for polypeptides made of five residues and investigate the length dependence of the rates. We examined the refolding of a 21-residue structure. The results are compared with the predictions of an analytic model as well as molecular dynamics simulations. The 21-residue polypeptide results exhibit longer timescales because of contributions from helix propagation from other sites in the structure. When denatured, the rates increase, reaching those of the five residue peptides. The complementary nature of the theoretical, experimental, and computational efforts gives a holistic and intuitive picture for this elementary biological process, which occurs on a feature-rich free energy landscape.

Results and Discussion

Helix initiation rates were measured via time-resolved fluorescence spectroscopy for three peptides: the alanine-based pentapeptide, Ac-W-A_3-H-NH_2 (Wh5); a glycine-based pentapeptide, Ac-W-G_3-H-NH_2 (Wgh5); and an alanine-based 21-residue helix, Ac-W-$(A)_3$H-$(A_3RA)_3$A-NH_2 (Wh21) (see Fig. 1). To ensure that the side chain of histidine was protonated, the peptides studied were made in acetate buffer at pH 4.8. The first two peptides were designed to have different helix content and stability due to the higher helix propensity of alanine over glycine (22). In addition, their minimal size means that helix initiation is the only process observed. Tryptophan serves as a sensitive fluorescence probe for the local structural change in these peptides, following the ultrafast T jump.

Steady-State Spectra. Fig. 2*A* displays representative far UV circular dichroism spectra of Wgh5 and Wh5. The results indicate that such short peptides do exhibit measurable helix formation in aqueous solutions. The alanine-based pentapeptide (Wh5) has a right-handed α-helical structure and the CD spectrum is in

Author contributions: M.M.L., O.F.M., G.S.J., and A.H.Z. performed research and wrote the paper.

The authors declare no conflict of interest.

[1]To whom correspondence should be addressed. E-mail: zewail@caltech.edu.

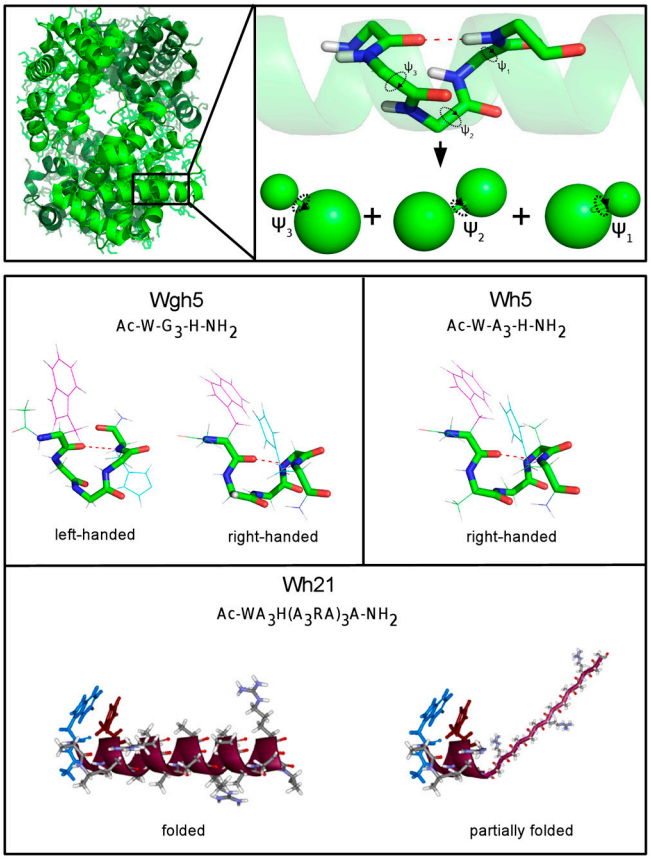

Fig. 1. Helix initiation. The three torsion angles of the memory-loss model that define the conformational state of a five-residue polypeptide backbone are labeled in (*Top*). The model maps the molecular content (both backbone and side-chain atoms) into effective van der Waals spheres on each side of a torsion angle. The helix initiation time is the characteristic time of all three torsion angles diffusing to the helical domain subject to thermal excitation and viscous drag on the effective spheres, at which point the structure is in the helical basin in the free energy landscape (see text). Structures of the Wh5 and both right- and left-handed structures of Wgh5 are given in the middle. Folded and partially folded structures of Wh21 are shown on the bottom. Tryptophan and histidine residues are located in the N and C termini of Wh5, Wh21, and Wgh5.

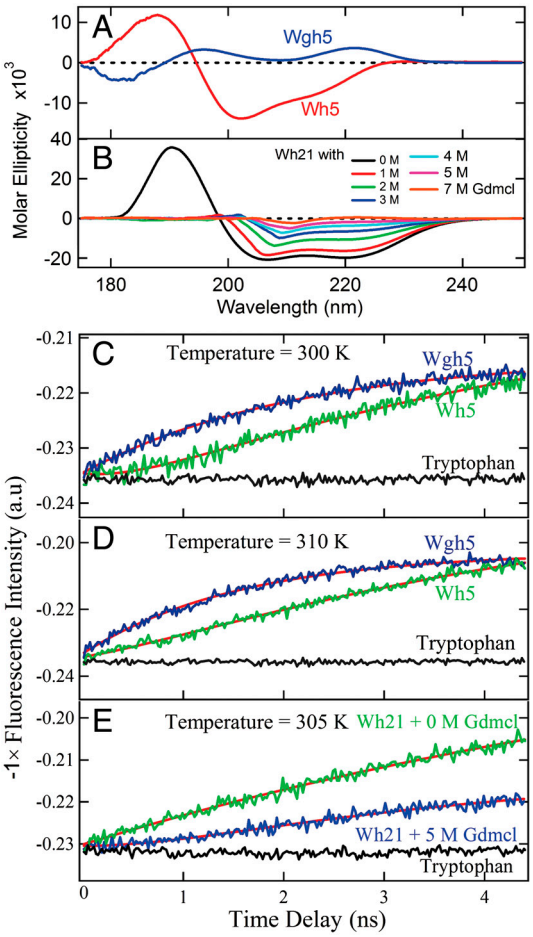

Fig. 2. Ultrafast *T*-jump transients and CD spectra. Far UV CD spectra of Wgh5 (blue) and Wh5 (red) at 266 K (*A*), display helix formation of these peptides in aqueous solution. (*B*) CD spectra of Wh21 as a function of guanidine hydrochloride concentration at room temperature. Transient evolution of the tryptophan fluorescence was monitored for Wgh5 (blue) and Wh5 (green) after ultrafast *T* jump to final temperatures (T_f) of 300 and 310 K over a time window ranging from $t = -50$ ps to $t = 4.4$ ns (*C* and *D*). The fluorescence signals are shown with negative amplitude in arbitrary units. For clarity, time zero is defined to be 50 ps after the *T* jump in order to only show the refolding relaxation dynamics. The initial heating is through the excitation of the overtone of the OH stretching vibration of water, inducing a 12 °C temperature jump, which means the initial temperature is $T_f - 12$ °C. Note that the signal of Wgh5 is rescaled to the intensity of Wh5 for clarity. Tryptophan was excited using an ultrafast UV pulse at 280 nm, and its fluorescence was monitored (310–500 nm). The measured fluorescence intensity is plotted in arbitrary units. (*E*) The transient evolution of the tryptophan fluorescence of Wh21 in acetate buffer at pH 4.8 with 0 M (green) and 5 M (blue) guanidine hydrochloride (GdmCl), following the *T* jump to 305 K final temperature. The flat black curve is the fluorescence of the free tryptophan in water under identical conditions, following the *T* jump, which is used as a baseline. All experiments were performed in acetate buffer at pH 4.8.

good agreement with those reported for short peptides and protein helices (23, 24). The glycine-based pentapeptide (Wgh5), on the other hand, produces a dominant left-handed helix signature, similar to the left-handed helix spectrum reported for D-amino acid peptides (25); however, although the left-handed helical population is dominant, the structures we probe for Wgh5 are those of right-handed helices because the strong tryptophan-histidine quenching mechanism is sterically suppressed in the left-handed helix because of backbone hydrogen bonding (see Fig. 1). The percent of helix formation from CD measurements was found to be 20 ± 5 and 5 ± 2 at 310 K for Wh5 and Wgh5, respectively, and the fluorescence signal in the *T*-jump experiments clearly reflects the decrease in right-handed helix concentration for Wgh5 when compared with Wh5. Shorter chain lengths were also formed by using the denaturing agent guanidine hydrochloride, and as shown in Fig. 2*B*, the spectrum of partially denatured Wh21 reaches that of Wh5.

Time-Resolved Fluorescence Spectroscopy. The peptide was heated using an ultrafast IR pulse centered at 1.45 μm, and the approach to the new equilibrium over time was monitored through the quenching of tryptophan fluorescence. Fig. 2*C* depicts a comparison of the observed kinetics over a time window ranging from $t = 0$ to $t = 4.4$ ns at 300 K for both Wgh5 (blue) and Wh5 (green) after applying the *T* jump. Note that, within the first 50 ps, the tryptophan fluorescence decreases dramatically due to the temperature rise resulting from the water thermalization (21). The unfolding and solvent relaxation (solvation) events indeed occur during this time window and cannot be resolved, and it is only after this time window that the conformational diffusion rate equilibrates to the final temperature, leading to an additional quenching (decrease) in the tryptophan fluorescence by histidine while the peptide searches for the helical structure. For this reason and clarity, time zero is defined to be 50 ps after the *T* jump in order to only show the refolding relaxation dynamics. The relaxation profile of Wgh5 is described by a single-

exponential function, whereas for Wh5, a double-exponential function was invoked. The corresponding time constants are as follows: 2.2 ± 0.3 ns for Wgh5, and 0.85 ± 0.3 ns (τ_1) and 5.3 ± 1.9 ns (τ_2) for Wh5. These observations indicate the importance of sequence on folding behavior even at the smallest scale of length. In the case of Wh5, the steric hindrance of the CH_3 side chains is the key for separation of torsional diffusion from local annealing, whereas the absence of such hindrance in Wgh5 because of the hydrogen side chains leads to a single-exponential profile for the entire helix initiation process.

The temperature dependence of helix initiation was also studied. At higher temperatures, the rate of helix formation increases: At 310 K, the measured time constant for Wgh5 is 1.4 ± 0.2 ns, whereas for Wh5 they are 0.65 ± 0.25 ns (τ_1) and 4.7 ± 0.6 ns (τ_2) (Fig. 2*D*). This trend is consistent with the diffusion being the rate-limiting step (see below). In the case of Wh5, the fast component contributes about 10–20% depending on the final temperature, and the error bar in τ_2 is large because of the short time window. For this reason, we performed the experiment at higher temperature to identify the asymptotic level of the recovery, and thus determined that the quoted errors are reasonable. From these dynamics, we can infer that the process is at least three-state, and because the fast time constant has a much smaller amplitude than the slow one, the rate-determining step is between the unfolded structure and the intermediate state or ensemble; this interpretation is borne out by the theoretical analysis (see below). It is worth mentioning that the asymptotic level of the recovery of Wh5 was found to be a factor of three lower at 330 K compared with the maximum value at 310 K, which is consistent with the relative helix content at those temperatures obtained from the CD data.

To investigate the role of peptide length in helix formation, specifically the additional contribution of helix propagation to the overall folding dynamics,*T*-jump relaxation measurements were also performed on the 21-residue α-helical polypeptide Wh21 in the presence and absence of a denaturant. Fig. 2*E* (green) displays a fast component of the relaxation process of Wh21 at a final temperature of 305 K. Although Wh21 is a well-studied system (8), this evidence for the existence of a few nanoseconds transient behavior was previously undocumented. When comparing with the subnanosecond fast process measured for Wh5, it is concluded that the measured rates are associated with backbone conformational dynamics, despite the identical location of the tryptophan and histidine residues in the two structures.

The effect of denaturing agent on these results is dramatic. Fig. 2*E* (blue) shows the ultrafast kinetics trace of Wh21 following the *T* jump to 305 K final temperature in 5 M guanidine hydrochloride. The transient displays double-exponential behavior with the characteristic time constants of 0.8 ± 0.3 ns (τ_1, 15%) and 2.8 ± 1.0 ns (τ_2, 85%), thus mirroring the temporal behavior of Wh5, which is identical to the first five residues of Wh21. It follows that the propagation of helicity from nonlocal parts of the structure in the absence of denaturant convolutes the elementary (intrinsic) nature of the dynamics.

Coarse-Grained Model. These experimental results of sequence, temperature, and length dependencies elucidate the nature of the processes involved in folding. The fast relaxation dynamics, which takes place within a few hundred picoseconds, is on the same timescale as the ultrafast hydrogen-bond breaking/formation (which requires backbone annealing) between the C = O group of the tryptophan at position 1 and the N-H group of histidine at position 5 (26). The observed double-exponential behavior of Wh5 with well-separated time constants indicates that helix initiation for Wh5 is not a two-state process. MD simulations on short peptides have in fact identified locally stable intermediate(s) that arrange to the compact structure (27). On the other hand, the observed single-exponential behavior for glycine-based pentapeptide (Wgh5) does not necessarily mean that the folding is a two-state process because multiple components with similar timescales may not be experimentally separable. For this reason, we formulated the following coarse-grained diffusion model and also carried atomistic MD ensemble-convergent simulations for our structural dynamics.

The model separates the timescale into two regimes: a slow noncooperative diffusive search over the collective degrees of freedom to find the helical basin in the free energy landscape, and a fast cooperative annealing to the native state within the helical basin. It is assumed that the characteristic time to surmount the steric barrier to escape the helical basin is longer than the annealing time but shorter than that of torsional diffusion. This assumption is supported a posteriori by MD simulations (see below). The concept of the helical basin within the energy landscape casts the rate-limiting step of the *continuous* diffusion of three angles into a *discrete* problem involving the number of trials necessary to observe three independent events. As such, we show below that rotational diffusion sets a well-defined τ, which is characteristic of the time between trials.

The polypeptide is modeled as a chain linked by a set of torsion angles, two for each of three residues that lie between the hydrogen bond (Fig. 1, *Top*). Thus one full turn of the α-helix is determined by three pairs of backbone torsion angles (φ_1,ψ_1), (φ_2,ψ_2), and (φ_3,ψ_3). In order to form the helix, all three sets of torsion angles must be in the helical configuration. We define the structure to be in the helical basin when all torsional angles are in the right-handed helix domain of the Ramachandran diagram, after which fast annealing can occur. Because φ is always in the helical range (see below), the rotational diffusion problem is reduced to the probability of finding all three values of ψ to be in the helical domain. Therefore, the helix initiation time, t_{init}, can be expressed as $t_{\text{init}} = \tau/p^3$, where τ is the characteristic time for the degrees of freedom to thermally diffuse to an uncorrelated backbone configuration (i.e., memory loss) and p is the probability that each degree of freedom is in an α-helical domain. Note that torsional ("conformational") diffusion is the superposition of three modes of rotation, and that the rotating masses are shared between modes (Fig. 1, *Top*).

The dihedral angle ψ is defined by the relative rotation of the bodies (modeled to first order as spheres) on either side of the bond in a viscous Brownian temperature bath. Thus the autocorrelation time, τ, is the temporal decay time of the ensemble average of $\cos\psi$, denoted by $\langle\cos\psi\rangle$. Because random diffusion is time-translation invariant, the correlation $\langle\cos\psi\rangle$ decays by the same factor at every time step—i.e., $\langle\cos\psi\rangle = e^{-t/\tau}$. This exponential decay naturally defines τ as the unique randomization time of the peptide conformation. Expanding both sides of this relation and matching the first-order term for early times, we obtained $\langle\psi^2\rangle = 2t/\tau$. Free rotation with respect to the dihedral angle ψ is equivalent to independent rotation of the two spheres on each side of the bond, denoted by θ_a and θ_b. Accordingly, $\langle\psi^2\rangle = \langle{\theta_a}^2\rangle + \langle{\theta_b}^2\rangle$. From Einstein's equation of diffusion in one dimension (which is valid for rotational diffusion at early times) (28), $\langle\theta\rangle = 2kTt/\gamma$. Here k, T, and γ are the Boltzmann constant, temperature, and coefficient of friction, respectively. Substituting this expression for $\langle\theta^2\rangle$ and then $\langle\psi^2\rangle$, one finds τ to be $\gamma_a\gamma_b/kT(\gamma_a + \gamma_b)$. For a sphere of volume V rotating in a fluid with viscosity η, Stokes obtained $\gamma = 6\eta V$ (29). Therefore, the initiation time can be written in terms of the temperature T, the viscosity of water η, and the volumes of the rotating masses on either side of each bond ($V_{a/b}$, which is similar for all three bonds): $t_{\text{init}} = 6\eta V_a V_b/p^3 kT(V_a + V_b)$.

Recently, the classic Ramachandran (30) steric plot was updated by Ho et. al (31) to reflect the empirical dihedral angle distribution. As in the original plot, there is a weak steric barrier separating the right-handed α-helix domain from the β-strand domain. According to the (non-glycine/proline) map, reproduced in

Fig. 3 (*Top, Inset*; note that the dark blue regions have no steric clashes), the right-handed α-helical domain spans all allowed φ values and about half of allowed values of ψ, neglecting the much smaller left-handed helix region, which is isolated by a significant steric barrier (31). Therefore, $p \approx 1/2$, and the initiation time is given by

$$t_{\text{init}} = \frac{\tau}{p^3} = \frac{48\eta V_a V_b}{kT(V_a + V_b)}.$$

For helix initiation in the interior of a long polypeptide, V_a and V_b should be chosen to be the volume of the Kuhn length of the chain, which for proteins is typically about 3–4 residues long (32). Thus, the spherical approximation is reasonable even for helix initiation in the interior of long proteins, with the initiation rate about three times slower than at the protein ends because of the increased values of $V_{a/b}$. The above equation will be used to calculate helix initiation rates and we will compare the results obtained with those rates measured via the T-jump methodology and with all-atom MD simulations.

For Wh5, the slowest rotating dihedral angle is ψ_2, with $V_a = 323$ Å^3 and $V_b = 232$ Å^3 assuming no hydration layer. The effective volume assuming one or two layers of water bound with varying tightness to the surface (typical for proteins) can be estimated using the van der Waals water diameter of 2.82 Å (33). At $T = 293$ K, the viscosity of water $\eta = 0.001$ Ns/m^2 (34), for which $t_{\text{init}} \approx 5$ ns for one effective layer of bound water. For a range of temperatures, t_{init} is plotted in Fig. 3 (*Top*) with various degrees of hydration along with the experimental T-jump results for Wh5. Because the solvation shell is typically 1–2 layers thick (35), the predicted initiation rates agree with the measured values to within a factor of two. Note that the main effect of the temperature is via the temperature-dependent viscosity. This order-of-magnitude estimate is surprisingly good given the neglect of the effect of shape and intramolecular interactions. Nevertheless, the model description of cooperative diffusion can accurately account for helix initiation. In addition, the temperature dependence (slope) of the folding time is consistent with the experimental results for all measurements reported here.

Computational. MD simulations were performed to further confirm the assumptions and predictions of the analytic model and to explain the higher-order details of the experimental time-dependent data: namely, the double- and single-exponential refolding times of Wh5 and Wgh5, respectively. Molecular construction and MD simulations were performed using the CHARMM suite of programs and the CHARMM22/CMAP force field (36–38). For Wh5/Wgh5, the structure was centered in the cubic primary-simulation cell with initial box length of 30.0/28.5 Å. MD simulations were performed using periodic boundary conditions at 311 K in order to mimic the conditions following a 13° T jump. The starting structures of both polypeptides were constructed with random backbone configurations and the same end-capping as for the experiments. One hundred separate independent trajectories, each lasting 100 ns, were obtained in order to yield a total simulation time of 10 μs for each peptide.

At every picosecond frame of the trajectory, the rmsd of the backbone from that of a canonical α-helix was calculated. All frames within 0.7 Å were considered to be α-helical because 0.7 was the upper envelope of the well-defined rmsd basin corresponding to the α-helix structure in the simulations. Based on this rubric, the percent of right-handed helix content at 311 K was 20% and 3% for Wh5 and Wgh5, respectively. The percent of left-handed helix content for Wgh5 was 6%, in agreement with the CD results favoring the left-handed helix.

For each instance of helix initiation, the folding time is defined to be the elapsed time between an unfolding event and a refolding event. The total number of independently obtained folding times of the right-handed helix was 595 and 244 for Wh5 and

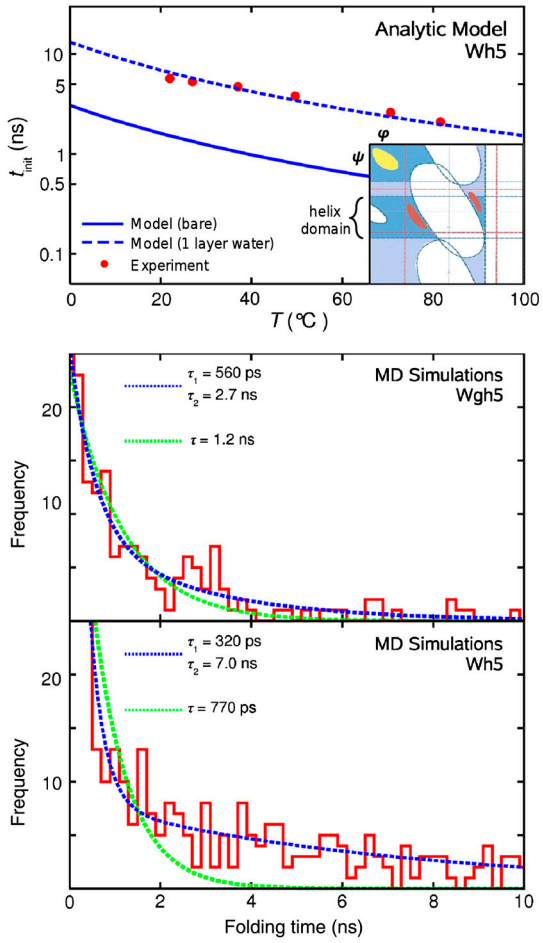

Fig. 3. Theoretical and computational results. The helical and nonhelical domains used in the model are taken from the corresponding regions of the updated (non-glycine) Ramachandran plot of Ho et. al (31) (*Top, Inset*). The α-helix regions (both left- and right-handed) are shown in red and the β-strand region is shown in yellow. Note that each region is within a larger sterically unrestricted domain (dark blue). Whereas crossing between right-handed helix and β-strand domains requires traversing a region of minimal steric strain (light blue), the left-handed helical domain is separated by a region of substantial steric strain (white). The predictions of the model are compared with the experimental results for Wh5, showing helix formation rates predicted by the analytic model with ultrafast T-jump experiments for Wh5 as a function of temperature (*Top*). Regardless of the extent of solvation, the predicted rate maintains the same temperature dependence as the experimental results. MD results showing the histogram distribution of folding times for Wgh5 (*Middle*) and Wh5 (*Bottom*) are shown. The refolding statistics for Wh5 display two well-separated timescales, whereas those for Wgh5 indicate a single timescale. Significantly, the values of all fitted timescales are in good agreement with those measured experimentally.

Wgh5, respectively, allowing for an ensemble-level assessment of the folding process. As shown in the refolding distribution (frequency) plots in Fig. 3, both polypeptides display a range of refolding timescales from hundreds of picoseconds to nanoseconds. For Wh5, the distribution of folding times fits closely to a double-exponential function and poorly to a single-exponential function. The two time constants, 320 ps and 7.0 ns, are in good agreement with those found experimentally at the same temperature. For Wgh5, the quality of a single-exponential fit is comparable to that of the double-exponential fit, yielding a single time constant of 1.2 ns, again in good agreement with the single-exponential time found experimentally. The trajectories indicate that the experimentally measured rates on the shorter timescale correspond to hydrogen-bond formation and local structural perturbations, whereas those on longer timescales correspond to conforma-

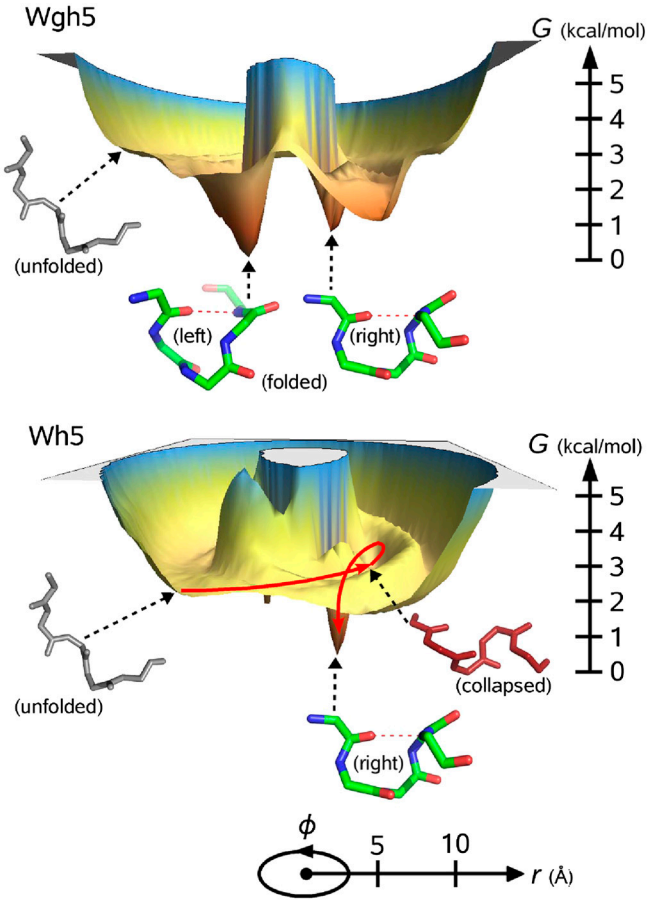

Fig. 4. Results-based free energy landscapes. The landscapes are parameterized in polar coordinates using the hydrogen-bond distance and overall twisting angle (see text). (*Upper*) The landscape for Wgh5 shows the existence of both left- and right-handed helices (green structures), with the left-handed helix more stable. (*Lower*) In contrast, the landscape of Wh5 shows only the right-handed helix with a steric wall separating the helical domain from the unfolded state. The dominant pathway is defined (red arrow) by a slow diffusion from the unfolded state (gray structure) to the helical domain (red structure), followed by fast annealing to the helical (green) structure.

tional diffusion from a random coil structure. Conformational diffusion is faster for Wgh5 than Wh5 because of the decrease in both viscous drag and steric clashes of the smaller glycine side chains. For Wgh5, the overlap in time of local annealing and global diffusion resulted in single-exponential time dependence, in agreement with the experimental findings.

We now can construct the free energy landscapes of the (un) folding dynamics from the results of the ensemble-convergent MD simulations, as depicted in Fig. 4. Each point on the landscape is parameterized by the polar coordinates (r,φ), where r is the oxygen–nitrogen distance between residue 1 and residue 5 (1O–5N), and φ is the torsional angle defined by 1O-2C$^{\alpha}$-4C$^{\alpha}$-5N. These order parameters allow for an intuitive visualization of the peptide conformation space, where r is the hydrogen-bond distance and φ is the overall backbone twist. The landscape is constructed by plotting the natural logarithm (multiplied by kT) of the fraction of time the polypeptide spends in the (r,φ) space; note that the total simulation time was sufficient to construct an ensemble-convergent landscape. For Wgh5 (Fig. 4, *Upper*), the landscape contains two minima with opposite twisting directions corresponding to the left- and right-handed helix. In addition to the greater stability of the left-handed helix, the landscape shows the lack of barriers separating the helical from the unfolded form. In contrast, the steric interactions of the methyl group side chains of Wh5 result in the existence of only the right-handed helix as well as the formation of a steric wall separating the helical domain from the unfolded domain (Fig. 4, *Lower*).

The memory-loss analytic model therefore captures the dominant folding mechanism in which the peptide undergoes the rate-limiting diffusive search to find the helical basin, after which the steric wall facilitates the fast search for the native helical structure before the peptide can diffuse out of the basin (Fig. 4, *Lower*). The model defines the role of the steric wall to separate the collective noncooperative torsional diffusion (the rate-limiting step) with cooperative annealing to the native state, and thereby the separation of timescales in the analytic solution. Without the existence of such a steric wall, as evident in the free energy landscape of Wgh5, the peptide can diffuse out of the helical basin, and helix initiation will no longer be separated into two temporal regimes. This landscape prediction is borne out by the experimental results.

Concluding Remarks. By using the *T*-jump methodology with picosecond temporal resolution, we have observed the folding of the shortest possible secondary structures, representing the speed limit of protein folding dynamics. Through studies of the sequence, temperature, and length dependencies of rates, together with the coarse-grained analytic diffusion model, as well as ensemble-converging atomistic simulations, a quantitative picture of the energy landscape emerges.This picture identifies the fast and slow processes of the dynamics with local and global conformational searches, respectively. The steric hindrance in Wh5 by the CH_3 side chains is the key element for the separation of the rate-limiting torsional (conformational) diffusion event from local annealing, whereas the absence of such steric frustration in Wgh5 leads to the overlap of these two processes, giving rise to a single temporal profile in helix initiation. These findings demonstrate the interplay of entropy and collective energetics in protein folding, even on the smallest length and timescales.

Materials and Methods

The peptides Ac-W(A)$_3$H-NH$_2$ (Wh5), Ac-W(G)$_3$H-NH$_2$ (Wgh5), and 21-residue helical heteropeptide Ac-WAAAH(AAARA)$_3$A-NH$_2$ (Wh21) were obtained from California Peptide Research with >98% purity. *N*-acetyl-L-tryptophanamide was >99% pure and was purchased from Sigma. Peptide concentrations were determined from the optical absorbance at 280 nm, using molar extinction coefficients of 5,690 M^{-1} cm^{-1}. Solutions were buffered with 20 mM sodium acetate at pH 4.8. A detailed experimental procedure for an ultrafast laser temperature jump setup has been described elsewhere (19). Here, we briefly present some of the modifications made. The near-IR signal and idler pulses were generated by two optical parametric amplifier systems pumped by a Ti:sapphire amplifier laser system operating at 800 nm (Spectra-Physics) with a repetition rate of 200 Hz. The *T*-jump pulse was set to 1.45 μm with a sufficient energy, typically 15–20 μJ at the sample.

In our MD simulations, in addition to the polypeptides, 872/747 transferable intermolecular potential 3-point water molecules and one chloride ion were added as a 61.5/71.7 mM salinity solvent, yielding an electrically neutral system comprising 2,698/2,314 atoms. The all-atom CHARMM22/CMAP force field was used for all calculations. To calculate helix refolding times, we define an unfolding event when the rmsd exceeds 2 Å and a refolding event when the rmsd drops below 0.5 Å for four consecutive frames (picoseconds), which was justified because 0.5 Å is the mean of the helical basin.

Note. In view of recent theoretical analysis, here we note the role of specific rates in the comparison between the experimental and theoretical findings of folding/unfolding. In the helix initiation *T*-jump experiments, and when the timescale of temperature rise is significantly shorter than that of the dynamics involved, caution must be taken regarding the use of simple kinetics (39) with the rates of folding and unfolding assumed to reach that of the final temperature during the entire temporal change, because the former involves the breaking of a single hydrogen bond, whereas the latter is the result of conformational diffusion. As a result, the observed helicity will not monotonically decrease, but rather "undershoot" and then rise to equilibrium; this kinetic behavior can be seen in diverse contexts as long as there are disparities in the equilibration of rates (40). In our experimental studies of helix-coil transitions, this behavior is what was observed (fast initial unfolding and slow refolding dynamics); the latter is evidenced in the decrease of

fluorescence, fluorescence quenching, as the tryptophan and histidine approach each other. Accordingly, the assumption of fluorescence increase (and master equation analysis) by De Sancho and Best (41) is inapplicable for this system. This point brings to focus the importance of careful analysis of the timescales involved in macromolecular dynamics.

ACKNOWLEDGMENTS. G.S.J. gratefully acknowledges Dr. Krzysztof Kuczera for helpful discussions. The authors are grateful to the National Science Foundation for funding this research at Caltech. M.M.L. acknowledges financial support from the Krell Institute and the US Department of Energy for a graduate fellowship at Caltech. Supported in part by Baylor University Undergraduate Research Grant (G.S.J.).

1. Onuchic JN, Luthey-Schulten Z, Wolynes PG (1997) Theory of protein folding: The energy landscape perspective. *Annu Rev Phys Chem* 48:545–600.
2. Callender RH, Dyer RB, Gilmanshin R, Woodruff WH (1998) Fast events in protein folding: The time evolution of primary processes. *Annu Rev Phys Chem* 49:173–202.
3. Daggett V, Fersht A (2003) The present view of the mechanism of protein folding. *Nat Rev Mol Cell Biol* 4:497–502.
4. Doshi U (2008) *Protein Folding, Misfolding and Aggregation, Classical Themes and Novel Approaches* (RSC Biomolecular Sciences, Cambridge, UK).
5. Liu F, Gruebele M (2008) Downhill dynamics and the molecular rate of protein folding. *Chem Phys Lett* 461:1–8.
6. Shaw DE, et al. (2010) Atomic-level characterization of the structural dynamics of proteins. *Science* 330:341–346.
7. Huang CY, Klemke JW, Getahun Z, DeGrado WF, Gai F (2001) Temperature-dependent helix-coil transition of an alanine based peptide. *J Am Chem Soc* 123:9235–9238.
8. Thompson PA, et al. (2000) The helix-coil kinetics of a heteropeptide. *J Phys Chem B* 104:378–389.
9. Gooding EAR AP, Wang JW, Palmer C, Fouts E, Volk M (2005) The effects of individual amino acids on the fast folding dynamics of alpha-helical peptides. *Chem Commun* 5985–5987.
10. Buchete NV, Hummer G (2008) Coarse master equations for peptide folding dynamics. *J Phys Chem B* 112:6057–6069.
11. Hummer G, Garcia AE, Garde S (2001) Helix nucleation kinetics from molecular simulations in explicit solvent. *Proteins Struct Funct Genet* 42:77–84.
12. Tobias DJ, Mertz JE, Brooks CL (1991) Nanosecond time scale folding dynamics of a pentapeptide in water. *Biochemistry* 30:6054–6058.
13. Huang CY, Getahun Z, Wang T, DeGrado WF, Gai F (2001) Time-resolved infrared study of the helix-coil transition using C-13-labeled helical peptides. *J Am Chem Soc* 123:12111–12112.
14. Wang T, Du DG, Gai F (2003) Helix-coil kinetics of two 14-residue peptides. *Chem Phys Lett* 370:842–848.
15. Gilmanshin R, Williams S, Callender RH, Woodruff WH, Dyer RB (1997) Fast events in protein folding: Relaxation dynamics of secondary and tertiary structure in native apomyoglobin. *Proc Natl Acad Sci USA* 94:3709–3713.
16. Williams SC TP, et al. (1996) Fast events in protein folding: Helix melting and formation in a small peptide. *Biochemistry* 35:691–697.
17. Dyer RB, Gai F, Woodruff WH (1998) Infrared studies of fast events in protein folding. *Acc Chem Res* 31:709–716.
18. Thompson PA, Eaton WA, Hofrichter J (1997) Laser temperature jump study of the helix reversible arrow coil kinetics of an alanine peptide interpreted with a 'kinetic zipper' model. *Biochemistry* 36:9200–9210.
19. Ma HR, Wan CZ, Zewail AH (2006) Ultrafast *T*-jump in water: Studies of conformation and reaction dynamics at the thermal limit. *J Am Chem Soc* 128:6338–6340.
20. Mohammed OF, Samartzis PC, Zewail AH (2009) Heating and cooling dynamics of carbon nanotubes observed by temperature-jump spectroscopy and electron microscopy. *J Am Chem Soc* 131:16010–16011.
21. Mohammed OF, Jas GS, Lin MM, Zewail AH (2009) Primary peptide folding dynamics observed with ultrafast temperature jump. *Angew Chem Int Ed Engl* 48:5628–5632.
22. Chakrabartty A, Schellman JA, Baldwin RL (1991) Large differences in the helix propensities of alanine and glycine. *Nature* 351:586–588.
23. Chin DH, Woody RW, Rohl CA, Baldwin RL (2002) Circular dichroism spectra of short, fixed-nucleus alanine helices. *Proc Natl Acad Sci USA* 99:15416–15421.
24. Sadqi M, de Alba E, Perez-Jimenez R, Sanchez-Ruiz JM, Munoz V (2009) A designed protein as experimental model of primordial folding. *Proc Natl Acad Sci USA* 106:4127–4132.
25. Mortishiresmith RJ, Drake AF, Nutkins JC, Williams DH (1991) Left-handed alpha helix formation by bacterial peptide. *FEBS Lett* 278:244–246.
26. Margulis CJ, Stern HA, Berne BJ (2002) Helix unfolding and intramolecular hydrogen bond dynamics in small alpha-helices in explicit solvent. *J Phys Chem B* 106:10748–10752.
27. Soman KV, Karimi A, Case DA (1993) Molecular-dynamics analysis of a ribonuclease C-peptide analog. *Biopolymers* 33:1567–1580.
28. Islam MA (2004) Einstein-Smoluchowski diffusion equation: A discussion. *Phys Scr* 70:120–125.
29. Bird RB, Stewart WN, Lightfoot EN (1960) *Transport Phenomena* (Wiley, New York).
30. Ramachandran GN, Ramakrishnan C, Sasisekharan V (1963) Stereochemistry of polypeptide chain configurations. *J Mol Biol* 7:95–99.
31. Ho BK, Thomas A, Brasseur R (2003) Revisiting the Ramachandran plot: Hard-sphere repulsion, electrostatics, and H-bonding in the alpha-helix. *Protein Sci* 12:2508–2522.
32. Toan NM, Marenduzzo D, Micheletti C (2005) Inferring the diameter of a biopolymer from its stretching response. *Biophys J* 89:80–86.
33. Franks F (2005) *Water: A Matrix of Life* (Royal Society of Chemistry, Cambridge, UK).
34. Sengers JV, Watson JTR (1986) Improved international formulations for the viscosity and thermal-conductivity of water substance. *J Phys Chem Ref Data* 15:1291–1314.
35. Svergun DI, et al. (1998) Protein hydration in solution: Experimental observation by X-ray and neutron scattering. *Proc Natl Acad Sci USA* 95:2267–2272.
36. Brooks BR, et al. (1983) Charmm: A program for macromolecular energy, minimization, and dynamics calculations. *J Comput Chem* 4:187–217.
37. MacKerell AD, et al. (1998) All-atom empirical potential for molecular modeling and dynamics studies of proteins. *J Phys Chem B* 102:3586–3616.
38. MacKerell AD, Feig M, Brooks CL (2004) Improved treatment of the protein backbone in empirical force fields. *J Am Chem Soc* 126:698–699.
39. Laidler KJ (1987) *Chemical Kinetics* (Harper & Row, New York), pp 35–39.
40. Frey PA, Hegeman AD (2007) *Enzymatic Reaction Mechanisms* (Oxford Univ Press, New York).
41. De Sancho D, Best RB (2011) What is the time scale for alpha-helix nucleation? *J Am Chem Soc* 133:6809–6816.